Eur. Phys. J. B **7**, 237–249 (1999)

THE EUROPEAN
PHYSICAL JOURNAL B
EDP Sciences

Shear banding instability in wormlike micellar solutions

M.M. Britton and P.T. Callaghan[a]

Institute of Fundamental Sciences-Physics, Massey University, Palmerston North, New Zealand

Received: 2 June 1998 / Received in final form and Accepted: 27 July 1998

Abstract. Using NMR velocimetry and mechanical measurements we study the flow dynamics, within a cone-and-plate rheometer, of the wormlike micelle system, cetylpyridinium chloride/sodium salicylate (CPyCl/NaSal) at 100 mM/60 mM concentration in distilled water. Depending on precise conditions within the system, two classes of behaviour are observed, one in which the boundary between different shear rate phases fluctuates rapidly (on the order of tens of milliseconds) and one in which it migrates slowly with a time constant of many seconds. These modes of behaviour may depend on minor solution impurities, which presumably affect the detailed constitutive properties, but also on the externally applied shear rate within a given system. We argue that the slow migrations are governed by stress relaxation effects while the rapid migrations are flow driven and arise from interfacial instability.

PACS. 61.25.Hq Macromolecular and polymer solutions; polymer melts; swelling – 47.20.Ft Instability of shear flows – 47.50.+d Non-Newtonian fluid flows

1 Introduction

In recent years there has been considerable interest in the rheological behaviour of those complex fluids which exhibit constitutive properties leading to flow instability. In particular there exists a class of fluids for which the intrinsic stress *vs.* strain relationship is non-monotonic in some sense, for example allowing multiple strain rate values at a given stress or *vice versa.* The classic example of such a system is the entangled polymer melt, or semi-dilute solution, which, in the predictions of the Doi-Edwards model of reptation dynamics [1,2], has a non-linear steady shear viscosity described by a stress which initially rises with increasing strain rate, but which reaches a maximum as shown in Figure 1, beyond which the stress reduces. This declining stress region cannot support stable flow so that the flow characteristics of such a fluid must be determined by the high shear rate branch, whose existence is required by the inevitable role played by higher frequency molecular dynamics, for example the underlying viscosity of the solvent in the case of semi-dilute solution, or the presence of Rouse, equilibration, or local segmental modes in the case of the polymer melts. Flow instability is believed to play a role in the so-called spurt effect [3], in the existence of a stress plateau in flow curves, and in the phenomenon of shear-banding in Couette flow [4–9]. Such bands are believed to be associated [10] with the co-existence of regions of different shear rate within the fluid. One common depiction of this processes is by analogy to a first order phase separation, in which the intersections of a stress tie line with the upper and lower branches of the underlying flow curve dictate the proportions of each band, as required to satisfy the average shear rate. The precise structure of such shear bands is a delicate theoretical problem.

In this article we shall focus on the shear flow characteristics of wormlike micellar solutions, a class of complex fluid which, in many respects, provides an ideal example of non-monotonic constitutive behaviour. In the semi-dilute regime the long, flexible, cylindrical micelles formed by a surfactant and counterion co-surfactant system, are believed to overlap and form an entangled network, thus experiencing reptation dynamics akin to polymer semi-dilute solutions. However, unlike the polymer case, where chain length polydispersity may result in a wide spectrum of relaxation times, the relaxation process in wormlike micelles is determined by a combination of reptation disengagement (τ_d) and breakage/recombination (τ_b) processes, and the effect of the rapid breakage/formation reaction process [11,12] is to pre-average any variation in the reptation time associated with polydispersity effects so that the characteristic relaxation time, τ is sharply defined by the mean value of $(\tau_d \tau_b)^{1/2}$. One consequence is a near-Maxwell behaviour in the linear response. In the reptation-reaction model of Cates [11,13] the non-linear flow curve for semi-dilute wormlike micelle solutions exhibits a stress which first rises and then falls with increasing shear rate, the critical shear rate at the maximum in the stress being [14] $\dot{\gamma}_c = 2.6/\tau_M$ while the stress maximum itself is $2G_0/3$, where G_0 is the high frequency plateau modulus as defined by the linear viscoelasticity. Note that the Maxwell time, τ_M, is defined in a macroscopic sense by η_0/G_0 where η_0 is the zero-shear viscosity.

---

[a] e-mail: `P.Callaghan@massey.ac.nz`

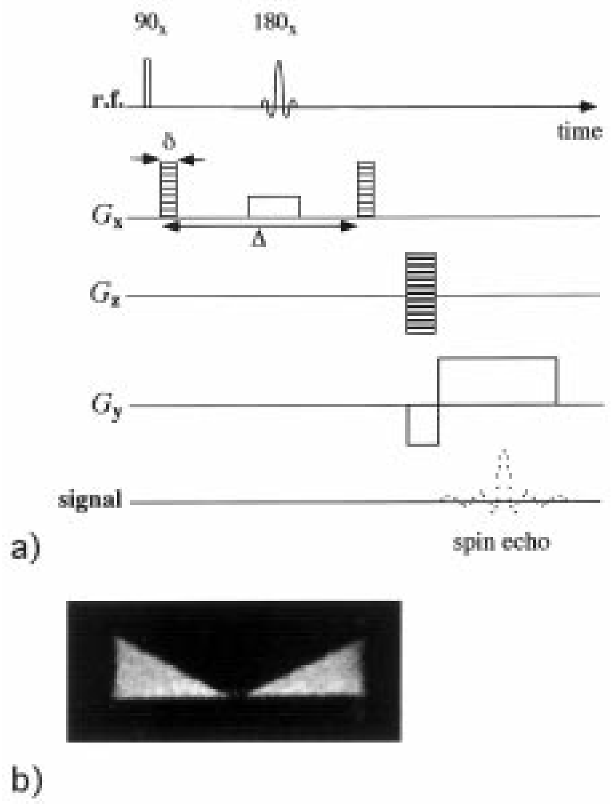

Fig. 1. (a) Schematic r.f. and gradient pulse sequence for standard velocity imaging with velocity encoding normal to the slice plane. The two narrow gradient (q) pulses of duration δ and separation Δ are increased in amplitude through 8 separate values in successive image acquisitions. (b) Proton spin density image from wormlike micelle solution in a 25 mm, 4° cone-and-plate system with a $\times 6$ vertical gain (pixel size of 195 μm, horizontal, by 32 μm, vertical). Note that the phase encode direction (vertical in the display) is coincident with the cone rotation axis and the main field axis.

Wormlike micelle systems not only manifest flow curves with wide stress plateaux, but in a number of these fluids, the associated phenomena of spurt and shear banding have been observed. Furthermore, both optical and neutron scattering experiments [4,15,16] have suggested an onset of shear-induced molecular ordering, analogous to the isotropic/nematic transition found in the equilibrium behaviour of liquid crystals. As a consequence these fluids provide an interesting platform on which to test the constitutive predictions of a well-defined molecular model, and with which to measure a wide range of parameters associated with molecular order and dynamics. However, it is also clear that there are many aspects of flow instability in wormlike micelles which are not well-understood. Some of these problems are intrinsic to the delicate assumptions which underpin the theories of flow in complex fluids, whilst others are particular to the molecular systems under study. In this latter category are time-dependence of the flow curve and the presence of relaxation processes much longer than the Maxwell time [16,17], the role of added salt (used to provide a screening of long range electrostatic interactions independent of the co-surfactant concentration [17]), the role of impurities in influencing the precise details of the flow dynamics, and the precise details of shear band structure, including whether these bands are broad or narrow [16,18], stable or unstable [8].

Underlying the various observations of shear banding phenomena are a range of theoretical issues which invite the following questions. Is the mechanism for shear rate selection under shear-banded flow driven by top-jumping or by stress coexistence governed by equilibrium conditions arising from the underlying constitutive equations and fluid dynamics? To what extent do the stress coexistence and the shear band structure depend on prior flow history and hence, do these arise from intrinsic constitutive properties or from the particularities of the fluid dynamics? What is the role of the gradient terms in governing the interfacial region between bands and will the shear rate profile be multi-banded or simply separated into two distinct regions? What is the role of flow geometry in determining band structure and what governs the position of any bands in the presence of heterogeneous stress? What determines the temporal stability of band structure? Can the separation into bands be viewed in terms of an order parameter, and in particular, in the case of wormlike surfactants is it associated with an isotropic/nematic transition, or is the separation associated solely with shear rate heterogeneity arising from the underlying hydrodynamic/rheological instability? Alternatively can the banding be viewed in terms of a non-equilibrium phase transition in multi-dimensional field variable space, in which separation by means of both shear rate and order parameter simultaneously occur [19]?

Here we focus on the issue of shear band stability and shear band structure in cone-and-plate flow of the wormlike micelle system, cetylpyridinium chloride/sodium salicylate (CPyCl/NaSal) at 100 mM/60 mM concentration in distilled water, a system originally investigated by Rehage and Hoffman [20]. At this concentration ($\phi = 4.5\%$ w/v) the zero shear viscosity, η_0, is well within the scaling regime $\eta_0 \sim \phi^{3.3}$, indicating that the solution is semidilute and governed by reptative chain dynamics. At this particular ratio of surfactant/salt, Rehage and Hoffman found a maximum in η_0 and a single exponential relaxation process, consistent with Maxwellian linear viscoelastic behaviour.

In our own laboratory this same wormlike micelle system has been used in NMR microscopy studies of the spurt effect and shear banding in pipe, cylindrical Couette, and cone-and-plate flow [7,18,21]. By measurement of the velocity profiles under conditions of steady flow, we have been able to identify shear rate heterogeneity and measure the dependence of local shear rate on the average rate of strain within the fluid. Most recently we have shown [18] in cone-and-plate flow, that once the average shear rate exceeds $\dot{\gamma}_c$, this wormlike micelle system exhibits distinct shear bands, $\dot{\gamma}_{high}$ and $\dot{\gamma}_{low}$, with the high shear rate band centred within the gap and flanked by the two lower rate bands. Furthermore, on increasing the average shear rate the high shear rate band develops by increasing its width at constant local shear rate, $\dot{\gamma}_{high}$, consistent with the idea of a first order phase separation model.

Our previous NMR microscopy study [18] of the flow behaviour of this fluid under shear in a cone-and-plate system yielded the following results. First three bands were present, the central high shear band having two interfaces to adjacent low shear regions. Second, this band structure was largely independent of any imperfections in the cone alignment or in the positioning of the cone vertex with respect to the plate. Third, when the cone rotation speed and hence, the gap apparent shear rate, was increased the high shear rate band expanded in width at approximately constant maximum shear rate (around 60 s^{-1}) while the central high shear band had an interface, with the adjacent low shear regions of characteristic thickness which remained constant over a wide range of shear rates and central bandwidths. Finally, and of particular importance to the present study, we found that a consistent sharpness of the observed velocity distributions in each pixel, indicating that the measured shear-rate profiles were highly stable.

The finite width band in the cone-and-plate contrasted somewhat with the very narrow and intense bands found in cylindrical Couette flow [8,18]. Furthermore the value of the maximum shear rate, $\dot{\gamma}_{high}$, is substantially less than that found in cylindrical Couette and pipe flow, and substantially less that the value found at the onset of the high shear rate branch using mechanical rheometry. This discrepancy we had attributed to the highly uniform stress which exists within the cone-and-plate gap. A further finding of our earlier work was that there exist fluctuations in the flow profile of this surfactant system whose characteristic correlation times in the case of pipe flow, vary widely, according to average volume flow rate [8]. In the case of the cone-and-plate and cylindrical Couette geometries, where practical considerations limited us to a much narrower range of shear rates, we found that the band was highly stable in the former case, and slowly migrating, on the timescale of minutes, in the latter.

In the present article we show how the NMR method may be used to investigate flow stability on the timescale from the milliseconds to minutes and relate the observed fluctuations directly to the mean shear rate profile. Furthermore, we investigate the degree to which the observed band structure is dependent on prior flow history, obtaining velocity profiles at closely spaced intervals under a range of startup conditions.

Recently, we have become aware that quite subtle changes in the fluid composition can radically alter the nature of the fluid banding even within the same cone-and-plate apparatus, and in particular, that the key to understanding that band structure lies in the nature of the fluctuations which are present. In what follows we will show the range of band structures possible and how these are exquisitely sensitive to the sample composition. In doing so we will correlate our findings with the flow curve data obtained using mechanical rheometry.

2 Experimental

The cone-and-plate cell used to shear fluids within the radiofrequency coils of our NMR probehead has been described in detail elsewhere [22]. Both the cone and plate are made out of the machinable ceramic MACOR (Corning, NY) and we have used two cones, with angles of 4° and 7°, the cone diameter being 24 mm or 16 mm in each case. A range of step-down gearboxes connect a remotely-controlled stepper motor to the drive shaft which, in turn, is connected to the cone axis through the room temperature (25 °C) bore of the 7 T superconducting magnet. The mean apparent shear rate within the gap of the cone-and-plate is given by $\omega/\tan\alpha$ where ω is the angular speed of the cone and α is the gap angle. This relationship was confirmed directly in experiments on Newtonian fluids [22] for which the shear rate within the gap is uniform.

The NMR velocimetry method used in this work relies on the use of a combination of magnetic field gradient pulses and resonant radiofrequency pulses which are used to phase-encode the NMR signal both for nuclear spin position as well as for translational displacement over a fixed time interval, in the range 10 to 1000 ms [23,24]. The data are then Fourier analyzed to provide a local velocity distribution for each pixel of the spatially resolved image, with velocity resolution on the order of 10 $\mu\mathrm{m\,s}^{-1}$ and spatial resolution of around $(20\ \mu\mathrm{m})^2$. It should be noted that the proton NMR signal is non-selective in a chemical sense and arises predominantly from the majority of the spins in the solvent water molecules.

We employ two approaches to selective encoding. In the first method, whose corresponding pulse sequence is shown in Figure 1a a planar slice of spins is excited and a two-dimensional image (128×128 pixels) of that plane is obtained, the total measurement time being typically 30 min. In the experiments reported here the slice thickness is 2 mm and the image plane is normal to the velocity-encoding direction. This thickness enables us to maximize our signal to noise by taking advantage of available symmetries, without introducing significant experimental artefacts. It should be noted that the slice selection process is always carried out in the centre of the velocity encoding period, so that only that motion which is normal to the slice axis is detected.

In all NMR microscopy experiments, spatial resolution must be traded against measurement time and image signal-to-noise ratios. Rather than increasing resolution in each dimension of the image plane, we are able to maintain sampling efficiency by enhancing the resolution along any axis of interest by means of a larger magnetic field gradient in that direction of encoding alone. This is an especially important facility when we wish to maximize our resolution across the cone and plate gap. Figure 1b shows an example of an image obtained in the 7 degree cone angle system in which the vertical gain is enhanced by a factor of 6. Note that no encoding for velocity is used and the intensity simply represents proton density in the fluid.

In a second experiment method (see Fig. 2a) in which we wish to follow temporal changes in the velocity

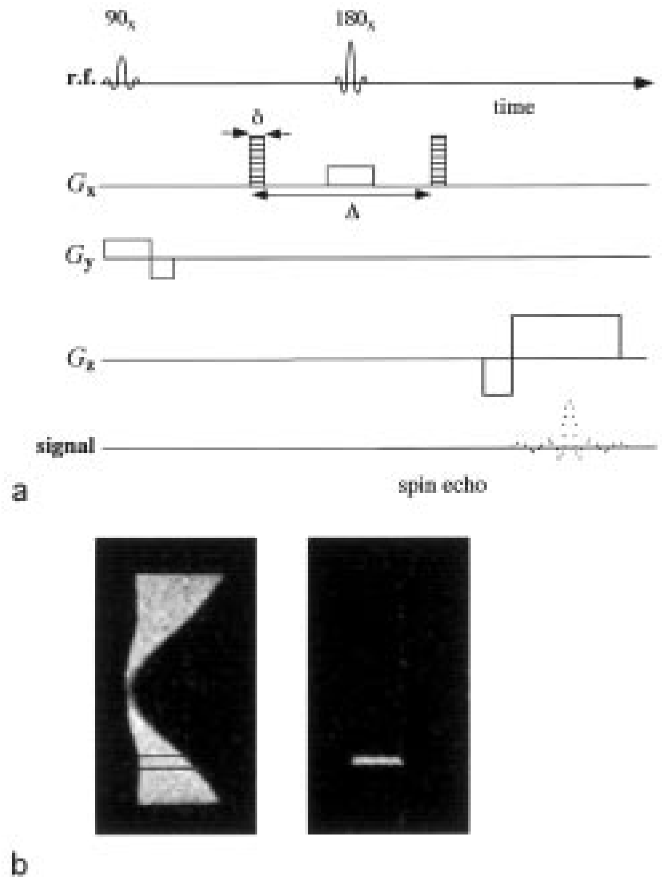

Fig. 2. (a) Schematic r.f. and gradient pulse sequence for 1-dimensional velocity imaging. The method of velocity encoding is the same as Figure 1a, except that the velocity image is read out along a 1-dimensional profile. (b) Spin density images for the whole gap (left) and the selected 1-d profile slice. These images were obtained in a 16 mm, 7° cone-and-plate system with a × 3 horizontal gain (pixel size of 156 μm, vertical, by 23.4 μm, horizontal). Note that the read out direction (horizontal in the display) is coincident with the cone rotation axis and the main field axis. This coincidence of the read out and main field directions leads to distortion due to susceptibility effects.

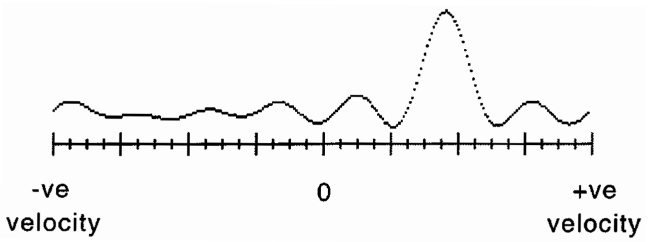

Fig. 3. Velocity distribution from a single pixel in a velocity image. The average fluid velocity is calculated from the offset of the peak from the origin, while the spread of velocities within the pixel, along with diffusion effects, determines the width.

distribution across the cone-and-plate gap over times much shorter than 30 min, we employ a one-dimensional encoding method, thus achieving a reduction by a factor of 128 in imaging time. This method relies on the excitation not only of a 2 mm layer of spins normal to the velocity, but, in addition, a selected subset of spins in an orthogonal 0.5 mm slice across the cone gap, as shown in Figure 2b. By this means we are able to read out the velocity distribution in each pixel of a one-dimensional profile across the gap, and at any preselected radius. It should be noted that the orientation of the image is chosen orthogonally to that shown in Figure 1, so placing the desired slice profile along the read-out direction. The spin density image of the whole gap now exhibits distortion of the fluid in the region near the cone apex. This occurs because of the coincidence of the polarizing field direction and the frequency-encoding (read) axis in this case. We ensured that the slice used for the 1-dimensional profile was selected at a position outside the affected area.

A crucial aspect of our method concerns the manner in which information concerning the fluid velocity in any pixel is acquired. The encoding utilizes the Pulsed Gradient Spin Echo method [23] in which the phase shift developed between two gradient pulses separated in time by Δ (see Figs. 1a and 2a), is directly proportional to the displacement, $\nu\Delta$, which the spins have undergone over that interval. Note that Δ can be as small as a few ms, or as long as the spin lattice relaxation time, around 1 s in our case.

Our method, by returning the velocity *distribution* for each pixel, provides an important range of information, as shown in Figure 3. First, the displacement of the distribution maximum gives us an indication of the mean velocity, while the width of the distribution tells us about fluctuations and the spatial heterogeneity of velocity within the pixel. This width will therefore be a convolution of the Gaussian arising from Brownian self-diffusion, the rectangular distribution arising from velocity shear across the pixel, and the additional contribution arising from any fluctuations on a timescale comparable with, or greater than Δ. In the case that the velocity field within the cone-and-plate varies very slowly over the total image encoding time of 30 min, we see a broad "smearing" of each pixel velocity distribution. Other structures may also arise, for example when the velocity field changes between two states, in which case the pixel velocity distribution comprises two distinct peaks. Such pixel velocity distribution structure gives an indication of slow fluctuations, on the timescale much longer than Δ (s) but shorter than the total image encoding time. These may then be further investigated by means of the one-dimensional slice method of Figure 2, since the much shorter slice imaging time of around 40 s allows such changes in the velocity field to monitored in real time.

In order to follow more rapid changes in velocity we employ a quite different approach, namely the pulse sequence shown in Figure 4. Here the velocity encoding is carried out using two PGSE pulse pairs applied in succession, each pulse pair imparting an opposite sign phase shift. Because the pairs are separated in time by an "exchange" time τ_{ex} they enable us to probe fluctuations

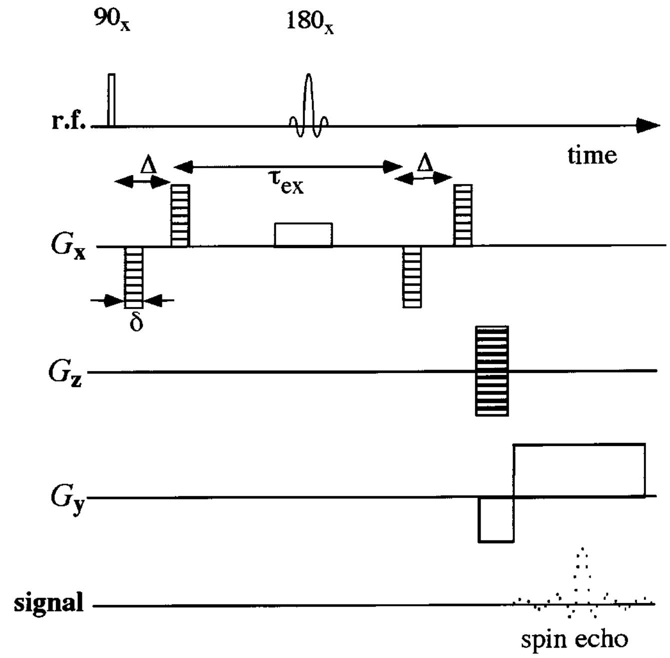

Fig. 4. Schematic double PGSE pulse sequence. Velocity encoding is carried out using two pairs of q pulses, which impart a phase shift of opposite sign. A stationary velocity field will result in a phase null and a velocity distribution centred at zero whose width is determined solely by diffusion. Fluctuations in the velocity field whose correlation times are shorter than or on the order of τ_{ex}, will be apparent *via* additional broadening.

on this timescale. In the case of a stationary velocity field, the resulting pixel velocity distribution is centred at zero velocity and has a width arising solely from microscopic molecular Brownian motion (correlation time $\ll \tau_{ex}$). In the case where there exists instability in the velocity field, any fluctuations on a time scale shorter than τ_{ex} will be detected *via* an enhanced distribution width. Since τ_{ex} may be varied in the range for 10's to 100's of ms, this approach is ideally suited to a monitoring of short time fluctuations. It is therefore complementary to the method outlined in the previous paragraph, which is applicable to fluctuations with correlation times on the order of a few seconds to several minutes.

Note that the use of double PGSE encoding of Figure 4 removes not only the effect of the mean velocity for the fluid in that pixel, but also that of velocity shear. By contrast the single PGSE method, used to measure the velocity map in the cone-and-plate, retains a significant shear contribution to each pixel velocity distribution. One consequence is that an image of pixel distribution widths provides a simple visualization of high shear regions of the gap during shear banding.

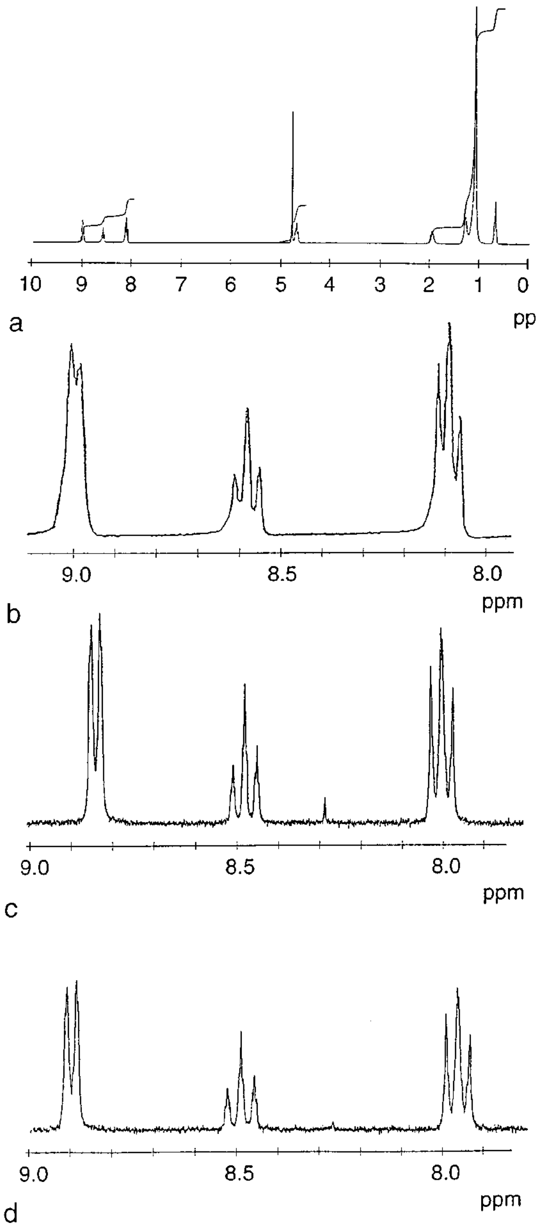

Fig. 5. Proton NMR spectrum for (a) batch 1 (BDH) with expanded spectra of the aromatic region for (b) batch 1 (BDH) (c) batch 2 (BDH) and (d) batch 3 (Sigma) cetylpyridinium chloride. All spectra were obtained in solution in D_2O using a Jeol GX270 NMR spectrometer.

The samples used in this work were prepared as follows. Four main sources of cetylpyridinium chloride were used. One was material synthesized in our own laboratory using the method described in the Appendix, one sample was obtained from Sigma (sigmaultra grade), and two others were different batches from BDH, one batch being obtained in late 1994 (batch number unknown), and the other being obtained in 1997 and with batch number: [21 285 235 505]. For future reference solutions made up with the '94 BDH material will be named batch 1, and solutions from the more recent BDH material, batch 2. Batch 3 solutions were those made out of the Sigma product. Proton NMR spectra, in solution in D_2O, for these materials are given in Figure 5. These were obtained using a Jeol GX270 NMR spectrometer at a ^{1}H frequency of 270 MHz. The proton spectra show that batch 1 is pure,

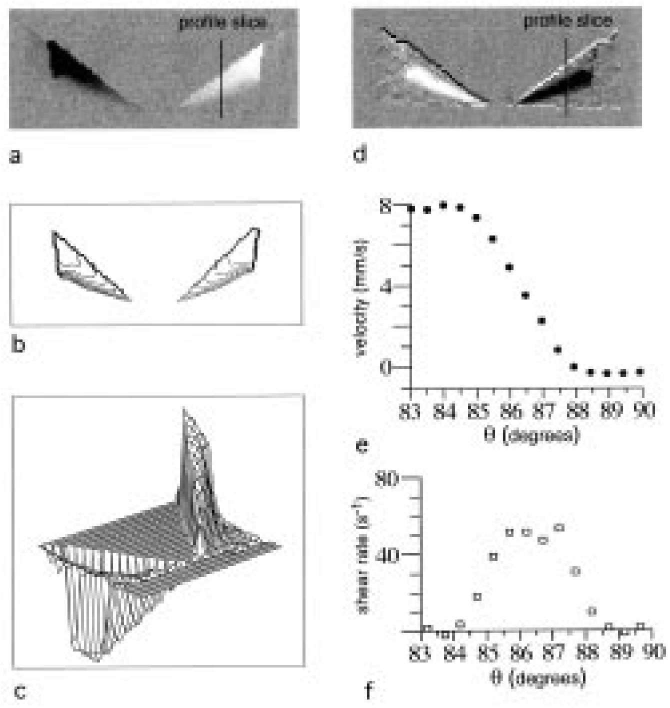

Fig. 6. (a) greyscale velocity image, (b) contour plot, (c) stack profile plot and (d) shear rate image for wormlike micelle solution (i) in a 16 mm/7° cone-and-plate system with a × 6 vertical gain (156 μm × 26 μm), at an apparent shear rate 17.5 s^{-1}. (e) and (f) are velocity and shear rate profiles for the vertical slice indicated in (a) and (d).

and that batches 2 and 3 display an extra peak around 8.3 ppm, indicating the presence of small amounts of impurities, the precise nature of which we cannot be certain.

The majority of experiments were performed on wormlike micelle solutions made out of the two BDH samples (batches 1 and 2). NMR velocimetry experiments were performed on a series of solutions of different ages (ranging from 5 days to 8 months). It was found that the age of the solution had no effect on the behaviour of the shear bands. To investigate the effect of temperature a series of solutions were stored at 20 °C, 25 °C and 60 °C for a short period of time (≈ 12 h) before the NMR velocimetry experiments. Again storage temperatures were found to have no effect on the behaviour of the shearbands in these solutions.

The effect of additional salt on these systems was also investigated. A solution using batch 2 material in 0.5 M brine was made, this system being similar to that used by Berret *et al.* [16] in their rheology study, although the ratio of cetylpyridinium chloride and sodium salicylate, used in our work, is slightly different, with a value of 0.6, compared to the value of 0.5 used in the Berret *et al.* study. Two less concentrated brine solutions were also made using both batch 1 and 2 material in 0.05 M brine.

A standard startup protocol was used for the velocity imaging experiments. For standard steady state velocity imaging, where a planar slice normal to the direction of flow is imaged over an experiment time of 30 min, the fluid would be sheared for 5–15 min before the experiment was started. Thus allowing the system to reach steady state. For the much shorter one-dimensional velocity encoding method, where we are interested in the "start-up" behaviour of the shearbands, a set of 8 NMR experiments were initiated immediately after the motor started to shear the fluid after the following delays: $t = 0$, 40 s, 110 s, 210 s, 370 s, 650 s, 1170 s, 2110 s.

All the rheometric data was collected at 25 °C on a Paar Physica UDS 200 rheometer using a 1° cone-and-plate system. A series of flow curves were obtained for all the above fluids and stress relaxation data following a sudden step in shear rate, were obtained at characteristic points on their flow curves. Frequency-dependent linear viscoelastic measurements were also carried out in order to obtain $G'(\omega)$ and $G''(\omega)$ for each of these systems.

3 Results

An example of a velocity (grey scale) map obtained in the wormlike surfactant system CPyCl/NaSal 100 mM/60 mM, is shown in Figure 6a in which the pixel resolution is 32.5 μm in the vertical direction and 195 μm horizontally. These data were obtained using a gap apparent shear rate in excess of $\dot{\gamma}_c$ and under these conditions significant shear bandings occurs. In Figures 6b and 6c the velocity field is represented respectively by a contour map and a stacked profile plot. The equivalent shear rate map is shown in Figure 6d, while Figures 6e and 6f show velocity and shear rate profiles taken across the gap at the radial position indicated.

3.1 Shear banding dynamics in the 100 mM/60 mM fluid (batch I)

The 100 mM/60 mM CPyCl/NaSal in distilled water system, made from the batch 1 CPyCl material, was used in our previously published study of shear banding in the cone-and-plate rheometer and for the purposes of the present article we shall refer to this as solution (i). In all the work with this system we have consistently found shear banding at gap shear rates above $\dot{\gamma}_c$, in which the fluid exhibits a broad central band of around 50 to 60 s^{-1} maximum shear rate. Figure 7 shows a progression of shear rate maps obtained at progressively higher shear rates, with corresponding shear rate profiles taken across these images along the path indicated. As the cone angular speed increases, these profiles broaden, at constant maximum, in accommodating the increasing average shear rate, a result consistent with the simple first order phase separation picture of [10]. And yet there exists an important discrepancy which can be seen by inspection of the flow curve for this material (see Fig. 3 in Ref. [21]) in which the upper shear rate branch occurs at a shear rate well in excess of 100 s^{-1}. Our observation of a shear band with magnitude 50 s^{-1}, is not strictly consistent with the

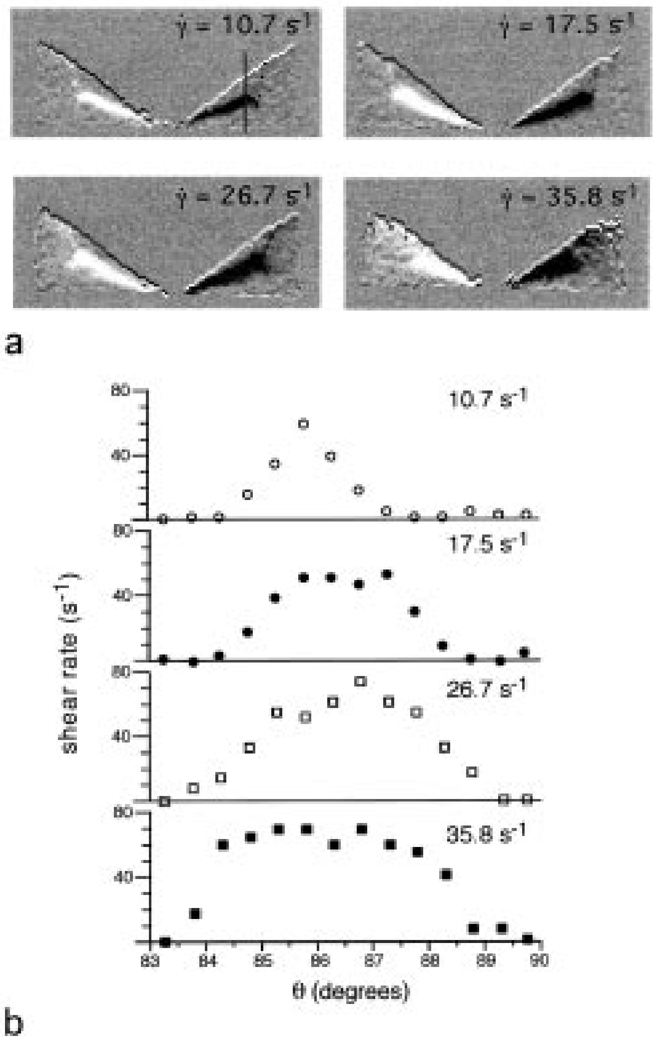

Fig. 7. (a) Shear rate images for solution (i) in the same system as Figure 6 at four different shear rates. (b) Shear rate profiles for the slice indicated in (a).

simple picture in which this band arises in a region of separated fluid phase, occupying a point on the upper branch of the flow curve. We are therefore led to enquire whether our shear band represents a region of pure high shear rate phase, or whether it comprises an admixture, in particular an admixture which arises because of underlying fluctuations.

In order to investigate the band dynamics we first inspect the pixel velocity distribution within the high shear rate band, an example of which is shown in Figure 8. This unique, and well shaped distribution indicates that if any fluctuations are present, then these must be considerably more rapid than the image encoding time, and probably on the order of the velocity encoding time, Δ. Indeed, to achieve a degree of motional narrowing of the pixel velocity spectrum would require fluctuations at the rate $\Delta\nu/\Delta x$ where $\Delta\nu$ is the change in velocity across the band and Δx is the range of migration. This value in the vicinity of $10\ \mathrm{s}^{-1}$, suggests a correlation time ≤ 100 ms. To test this hypothesis we have carried out a double PGSE encoding experiment at two different exchange times of 7 ms and 80 ms. Any fluctuation at a time much slower than τ_{ex} is expected to lead to a null result in which the pixel velocity distribution FWHM has its intrinsic value arising from molecular self-diffusion. This width will be common to all pixels in the image, irrespective of proximity to any shear band. By contrast, if the fluctuations occur on a time comparable with τ_{ex}, then distinct FWHM enhancement will result.

The results of the fluctuation experiment on the Batch 1 sample is shown in Figure 9. At $\tau_{ex} = 7$ ms no FWHM enhancement is seen while at $\tau_{ex} = 80$ ms dramatic enhancement exists, providing convincing evidence of velocity fluctuations at this timescale. Note that the FWHM maps of Figure 9 obtained using the double PGSE pair sequence are of a different character to that acquired using the single PGSE pair encoding, which will exhibit an enhancement, even under steady state conditions, provided that there exists a local velocity gradient. By contrast, that seen in Figure 9 can only arise *via fluctuations* and provides convincing proof of the role of such dynamics in the shear banding process.

3.2 Dependence of shear banding dynamics on impurities, on salinity and on concentration

The NMR velocimetry experiments carried out on the Batch 1 BDH material were also performed using the CPyCl synthesized by us, in the same (100 mM/60 mM) composition with NaSal in distilled water. The shear banding results were identical. However in repeating these experiments using material from a different origin, we have found quite different results. In order to elucidate these effects, we have carried out NMR velocimetry studies above $\dot{\gamma}_c$ on 6 other CPyCl/NaSal systems, namely solutions formed from (ii) Batch 2 at 4.5% w/v (100 mM/60 mM) in distilled water, (iii) Batch 2 at 5.0% w/v in distilled water, (iv) Batch 1 at 4.5% w/v in 0.05 M NaCl solution, (v) Batch 2 at 4.5% w/v in 0.05 M NaCl solution, (vi) Batch 2 at 4.5% w/v in 0.5 M NaCl solution, and (vii) Batch 3 at 4.5% in distilled water. We have particularly focussed on the differing behaviour of the Batch 1 and Batch 2 4.5% w/v distilled water systems (solutions (i) and (ii) respectively), carrying out scores of separate experiments on several preparations of the respective material. In particular we have studied these after allowing for differing times (5 days to 8 months after preparation). In all these measurements we have found a consistent discrepancy in the flow characteristics as measured by NMR Microscopy in the 7 degree cone-and-plate, a result which is graphically illustrated in the shear rate maps shown in Figure 10a for solution (ii), in Figure 10b for solution (iii) and in Figure 10c for solutions (v) and (vi). Note that the final figure shows data obtained at reduced gap magnification, although the cone angle is identical.

The shear banding phenomenon, whilst apparent for all gap shear rates above $\dot{\gamma}_c$, differs substantially in that

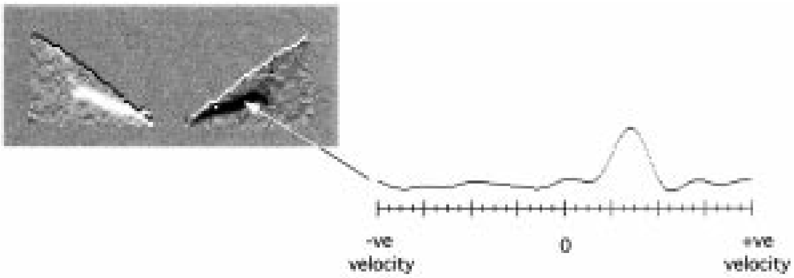

Fig. 8. Velocity image for solution (i) in the same system as Figure 6, at an apparent shear rate of 10.7 s^{-1}. The velocity distribution is given for a pixel inside the shear band, as indicated.

Table 1. Cetyl pyridinium chloride/sodium salicylate solutions used in this work.

solution	source of CPyCl	solvent	concentration (CPyCl/NaSal)	Maxwell time (/s) @ 298 K
(i)	Batch 1 (BDH)	H_2O	100 mM/60 mM	0.9
	own synthesis	H_2O	100 mM/60 mM	
(ii)	Batch 2 (BDH)	H_2O	100 mM/60 mM	1.9
(iii)	Batch 2 (BDH)	H_2O	111 mM/67 mM	1.4
(iv)	Batch 1 (BDH)	0.05 M $NaCl/H_2O$	100 mM/60 mM	0.12
(v)	Batch 2 (BDH)	0.05 M $NaCl/H_2O$	100 mM/60 mM	1.4
(vi)	Batch 2 (BDH)	0.50 M $NaCl/H_2O$	100 mM/60 mM	0.12
(vii)	Batch 3 (Sigma)	H_2O	100 mM/60 mM	2.6

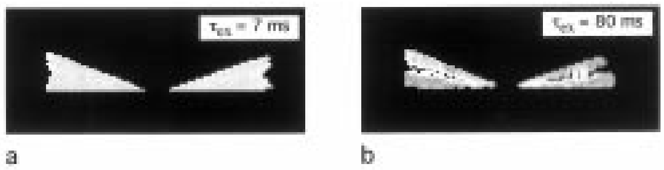

Fig. 9. FWHM image for solution (i) at an apparent shear rate of 14.3 s^{-1} in the 25 mm, 7° cone-and-plate system with × 3 vertical gain, obtained using the double PGSE pulse sequence shown in Figure 4 with exchange times of (a) 7 ms and (b) 80 ms.

the solution (i) material (Fig. 7) exhibits a broad central band of around 50 to 60 s^{-1} maximum shear rate, while the solution (ii) material (Fig. 10a) exhibits a narrow and much more intense band confined to a single pixel of our image over all accessible gap shear rates. However the width of this band is exquisitely sensitive to a small change in concentration, as in the comparison between Figures 10a and 10b, and to the presence of 0.05 M NaCl, as seen in Figure 10c. The addition of the salt has a similar effect on the Batch 1 solution, broadening the central high shear band so much that it occupies nearly all the space across the gap. It should be noted, that in all our work, the behaviour seen in these varied examples, was largely independent of cone angle, of misalignment in the cone and plate arrangement, and of the history of sample equilibration. Composition was the crucial factor determining the constitutive behaviour.

For the moment we focus on the solution (ii) data shown in Figure 10a. Because we cannot fully resolve this high shear rate band where it is confined to a single pixel, only the minimum possible value for this intrinsic maximum shear rate can be estimated. As the gap shear rate increases, the high shear rate remains single-pixel-narrow and intense and, based on our estimate from the largest apparent shear rates, we set this intrinsic maximum at around 100−150 s^{-1}. In order to investigate the stability of this band we have analyzed pixel velocity distributions in the vicinity of the band, as well as in the surrounding fluid on both the high velocity and low velocity sides. The results, which should be directly compared with the solution (i) data of Figure 8, are shown in Figure 11. Near the narrow but intense, high shear rate band of Figure 11, the velocity distribution is bimodal or smeared out, consistent

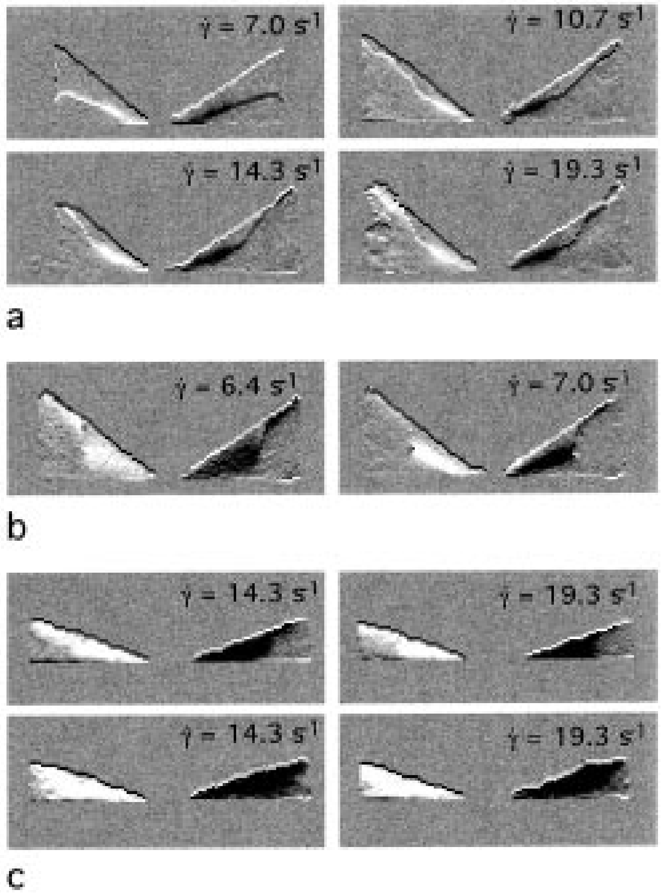

Fig. 10. Greyscale velocity images for (a) solution (ii) and (b) solution (iii) and (c) solutions (v) (top two images) and solution (iv) (bottom two images). The images obtained were in 16 mm, 7° cone-and-plate systems with a vertical gain in (a) and (b) of × 6 and (c) × 3.

with slow velocity field variations. It should be noted that the algorithm used to compute the velocity maps is based on locating the displacement from zero of the maximum in the pixel velocity distribution. Where a bimodal distribution occurs only the higher of the two peaks is found. However, a clue to the migration of this sharp band can be found in the velocity spectrum obtained in the vicinity of the shearband. The existence of two distinct peaks, one at high velocity and one at low velocity, suggests that the transition zone has wandered during the image acquisition, an interpretation which is supported by the existence of bimodal behaviour in a pixel adjacent to the band, but in which the dominant peak is the velocity which belongs to the low shear rate phase.

Clearly, any migration of the shearband in solution (ii), is too slow to motionally average the pixel velocity profiles, so that there exists the possibility to "capture" this movement in a one-dimensional imaging experiment in which the total encoding time is only 40 s. Figures 12a and 12b compares profiles across the gap for the Batch 1 and Batch 2 solutions in which four successive one-dimensional images are obtained, some time after startup. The Batch 2 solution clearly exhibits slow migration with a correlation time of several seconds, while the while the Batch 1 solution appears stationary, due to the much more rapid rate of fluctuation.

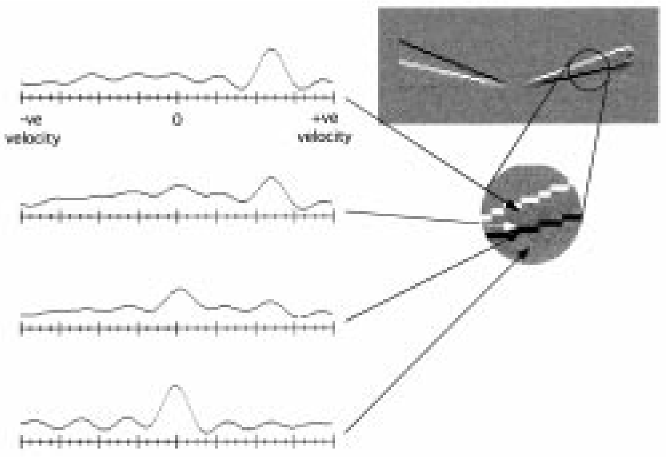

Fig. 11. Greyscale velocity image for solution (ii) in a 25 mm, 7° cone-and-plate system (× 3) at an apparent shear rate of 10.7 s^{-1}. Velocity distributions taken from different regions in the fluid, as indicated, are displayed. Note that upper bright lines are not shear bands but simply indicate the cone surface.

It is now clear that the differences between the apparent shear banding properties for the two systems lie in the dynamics of fluctuations, and that those dynamics are extremely sensitive to purity. We believe that the fundamental difference between the very different shear band structures apparent in the images of Figures 8 and 11 is simply that in the latter case the fluctuation is sufficiently slow that the NMR image provides a frozen view of the mode position, whilst in the former the migrations are sufficiently rapid that the pixel velocity distribution is motionally narrowed to produce a single peak position at the average velocity, in all of the pixels through which migration occurs. In both cases however the underlying shear band has a shear rate consistent with the high shear rate branch (*i.e.* > 100 s^{-1}). Our measurements also suggest that the same variation in the speed of fluctuations lies behind the broader shear bands found when the micelle concentration is increased, or when NaCl is added to the solution.

3.3 NMR velocimetry following startup

In order to follow the development of the shear band following startup, we have performed a number of one-dimensional imaging experiments in which the velocity profile along a chosen slice across the gap is monitored with time, following a sudden step in the average gap shear rate. In this work we have focussed solely on the Batch 1 and Batch 2 4.5% distilled water solutions (solutions (i) and (ii)) since these provide representative examples of the extremes of velocity fluctuation times found in this work. In the case of the Batch 1 material, for which the fluctuation correlation time was a few 10's of milliseconds, the stationary shear band was always established by

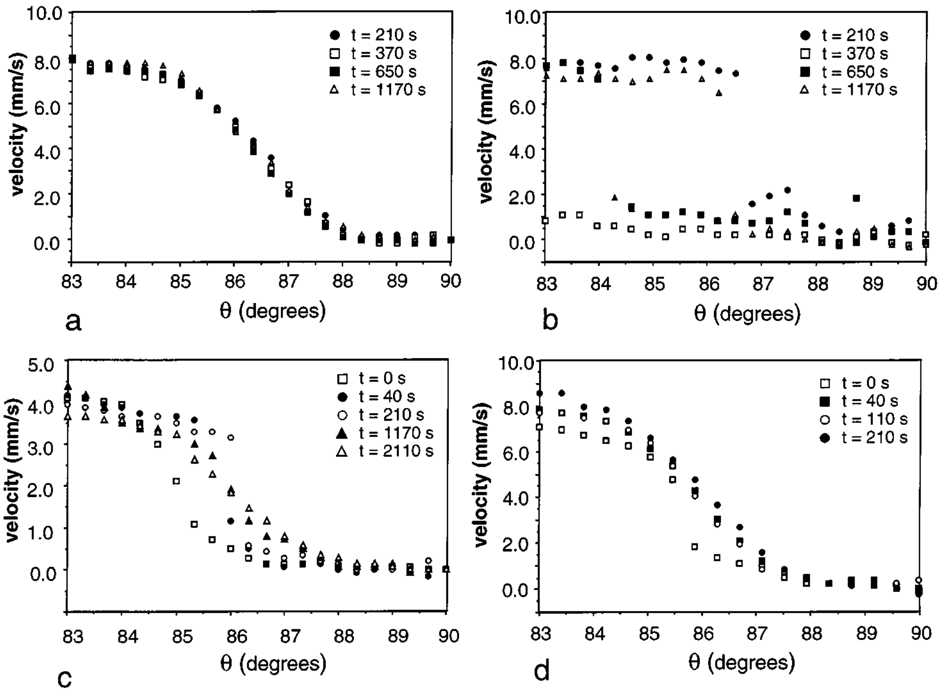

Fig. 12. Velocity profiles obtained using the 1-dimensional velocity imaging sequence for solutions (a) (i) and (b) (ii) over a series of time delays. Velocity profiles for solution (i) following shearing at 19.3 s^{-1} for some time and then a sudden step to (c) 7 s^{-1} and (d) 14.3 s^{-1}.

the first image, immediately after startup, irrespective of whether the startup was from rest, from a progressional increase in shear rate or when the direction of cone rotation is changed. In the case of the Batch 2 material, for which very slow shear band migrations are observed, these slow migrations always occurred, in apparently random steps over a wide range of the gap, irrespective of whether the startup was from rest, from a higher cone velocity, or from a negative cone velocity In short, the prior flow history appeared irrelevant following the time of around 40 s required to acquired the first image.

We note with interest that at low cone rotations speeds, a narrow shear band (*i.e.* one without rapid migration) can been observed for solution (i) and that a transition can be seen to the rapidly fluctuating state. Figure 12c shows a progression of 1-dimensional velocity images taken when the shear rate is suddenly set to 7 s^{-1} from below while Figure 12d shows the equivalent result when stepped from above. In both cases the final "steady state" corresponds to the broad band associated with rapid fluctuations. That such a sudden change in dynamics should be seen in this particular system under otherwise constant experimental conditions is strongly suggestive of a transition associated with instability.

3.4 Rheological measurements: Flow curves and stress relaxation

Figure 13 shows flow curves for the solution (i) to (vi) fluids obtained under controlled strain rate conditions. In each case the upper shear rate achieved was limited by fluid being expelled from the gap. These curves show a wide variation, the most surprising of which concerns the range found for the same 4.5% w/v distilled water system but with starting material, Batch 1 and Batch 2. One hint of a difference in the rheological properties of these two materials can be seen by comparing the flow curves of Figures 13a and 13b. In the latter case, a distinct peak is seen, an effect which we will show is due to a long time constant in the equilibration onto the steady state, an effect previously seen by Berret *et al.* [16] and by Grand *et al.* [17], who carried out experiments in which the fluid was rapidly taken from rest to a point on the flow curve and held at steady shear rate while the stress was monitored.

Because our NMR velocimetry data indicate the importance of fluctuations over timescales ranging from ms to many min, we are led to investigate more closely the role of equilibration processes relevant to the constitutive properties. Both Berret *et al.* and Grand *et al.* found a transient behaviour in which the shear stress relaxed to the equilibrium value with a time constant which depended on the degree to which the critical strain rate was exceeded. Near $\dot{\gamma}_c$ the time constants were many minutes whilst far above $\dot{\gamma}_c$ much more rapid decay was observed, although in no case was the relaxation time less than several seconds. Grand *et al.* were able to achieve exceedingly slow relaxation times, in excess of 1000 s, by holding the gap shear rate very close to $\dot{\gamma}_c$. It should be noted that these processes are all much slower than the Maxwell times for the fluids under study, a fact which Berret *et al.* ascribe to nucleation and growth processes in the presumed

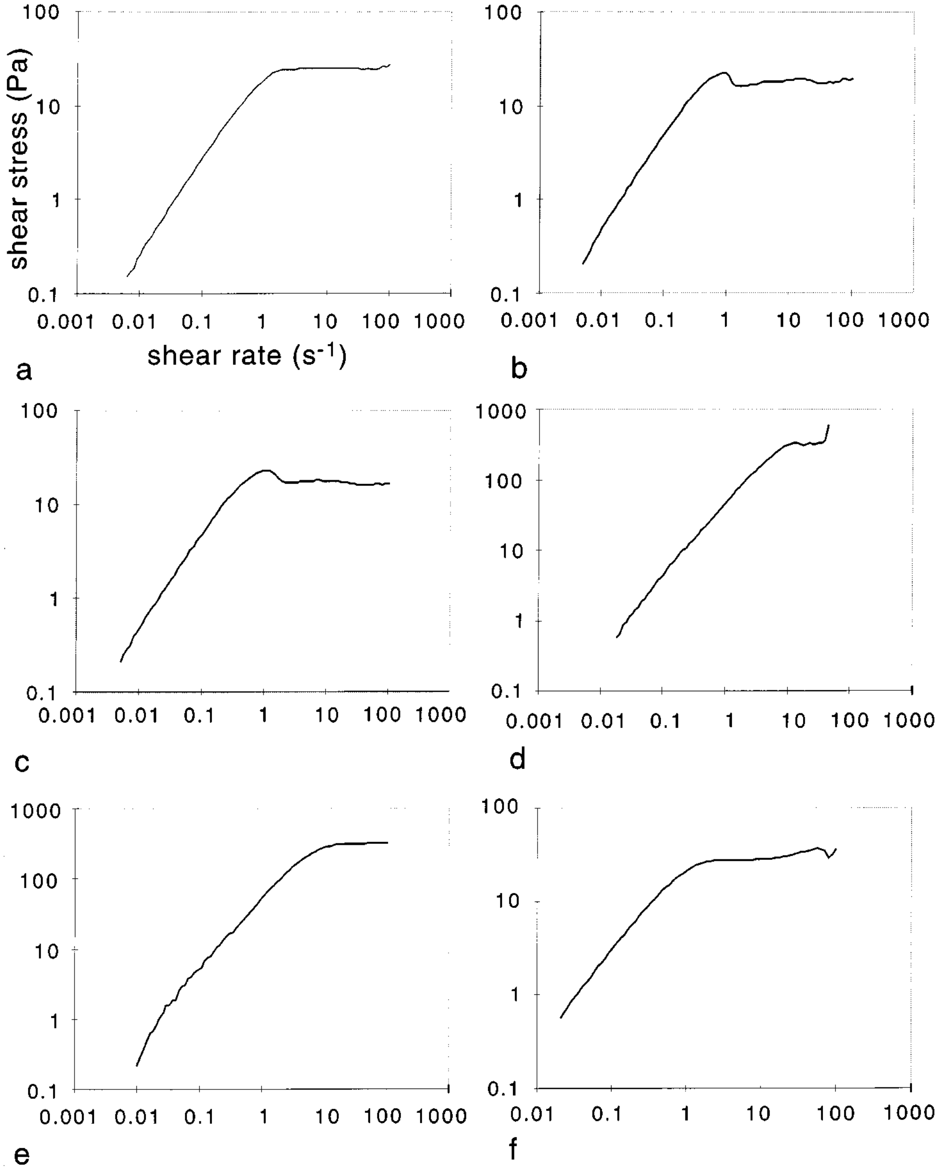

Fig. 13. Flow curves for solutions (a) (i), (b) (ii), (c) (iii), (d) (vi), (e) (v), (f) (iv) at 298 K.

isotropic/nematic phase transition, and which Grand *et al.* relate to the startup development of the shear flow in which the sharp band interface drifts from one position to another within the cell.

Figure 14 shows stress relaxation following startup to steady strain rate for the solution (i) and (ii) fluids at different values of the ratio $\dot{\gamma}/\dot{\gamma}_c$. As in the earlier experiments of Berret *et al.* and Grand *et al.*, we find that the stress relaxation at $\dot{\gamma}/\dot{\gamma}_c > 1$ becomes slower as $\dot{\gamma}/\dot{\gamma}_c$ approaches unity. Furthermore we note that the solution (ii) stress relaxation is somewhat slower than that found in solution (i) at similar values of $\dot{\gamma}/\dot{\gamma}_c$. This begs the question as to whether stress relaxation and shear band migration processes are related.

4 Conclusions

We have shown here that fluctuations in the flow behaviour of wormlike micellar solutions can lead to widely different apparent shear banding behaviour. In particular the structure of any observed shear band may well depend on the characteristic timescales of the observational technique employed. This may well explain some discrepancies in the literature concerning shear band structures in apparently identical systems. However, we have also shown that small impurity fractions, the presence of added salt, or a small variation on the concentration of the micellar surfactant itself, can drastically alter the system dynamics and hence the apparent band structure. This fact will be of crucial importance in comparing results obtained by different groups on the same system.

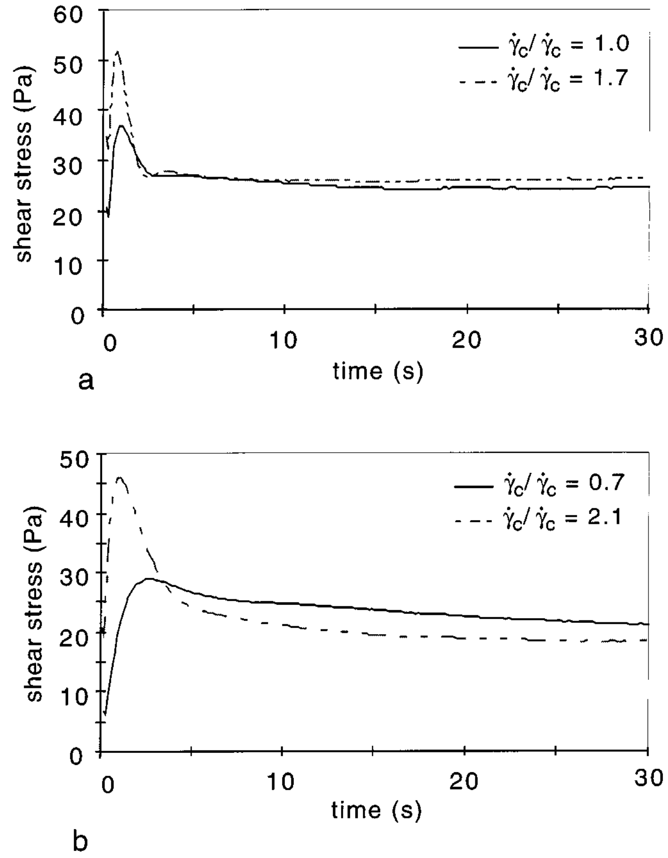

Fig. 14. Stress decay plots, at 298 K, for (a) solution (i) at shear rates of 3 s^{-1} and 5 s^{-1} ($\dot{\gamma}/\dot{\gamma}_c = 1.0$ and 1.7) respectively (b) solution (ii) at shear rates of 1 s^{-1} and 3 s^{-1} ($\dot{\gamma}/\dot{\gamma}_c = 0.7$ and 2.1).

We emphasize that the reduced average shear rate in the broad shear band exhibited in Figures 6, 7 and 8 cannot arise from an effect due to the limited pixel resolution of (20 μm)^2. For example, suppose that there co-existed many finely spaced, static high-shear-rate/low-shear-rate bands in the flow. In that case the velocity distribution obtained from a single pixel would exhibit two peaks, in contrast with that shown in Figure 8. Furthermore, the exchange experiment, for which the results are shown in Figure 9, would be devoid of effects due to fluctuations. In fact we can be certain that the averaging process which leads to the broad shear band is dynamic, and that the correlation time of the fluctuations is on the order of a few tens of ms.

It is well-known from theoretical studies that the factors which determine shear band structure and position are extremely delicate [25,26]. From this perspective it is not surprising that fluctuations in flow behaviour are observed. Such fluctuations are not confined to cone-and-plate flow but have also been observed in experiments involving wormlike micellar solutions in the pipe geometry [8,27]. Indeed, in an early paper on banded flow in pipes, McLeish [28] has pointed out that instability, under small perturbations to the shear band position, may well be a direct consequence of the inevitable discontinuity in the normal stresses at the interface between the high shear and low shear phases. In the McLeish picture material does not cross the interface and the boundary moves by ejecting or acquiring fluid of the two phases so that the separate volumes of each phase are conserved and the dynamics are governed by the flow. The driving force for the fluid transfer is the normal stress discontinuity. The stability criterion is subtle and depends on the flow geometry as well as on the fluid constitutive properties. We find this interdependence particularly interesting in view of the radial dependence of the fluctuation instability stability apparent in the solution (ii) data shown in Figure 10. Furthermore, the propagation speed for interface fluctuations is on the order of the fluid velocity. Given deformations on the order of the gap dimensions, this leads to correlation times less than $\dot{\gamma}_c^{-1}$ and quite consistent with the range of possible values found in the analysis based in Figure 9. We note that interface fluctuations have also been observed by Liu and Pine [29] in optical observations of fractured gels. In those experiments the fluctuation rate was again comparable with that expected given flow-driven perturbations.

Another mechanism for interfacial migration in the direction of the velocity gradient is by means of a local phase change in the adjoining fluid as material shifts between the low to the high shear branches of the flow curve. In the language of McLeish, this corresponds to material crossing the interface, in contrast with his model of fluid transport parallel to the interface, involving conservation of the separate volumes of each phase. In this case the instability criterion would be expected to be quite different and the time constants for fluctuation will be almost certainly be much longer, since they will be governed by the need for stress relaxation following a sudden change in shear rate, exactly the type of process which is represented in Figure 14. We are led to speculate that in solution (i) the fluid satisfies the McLeish criterion for instability while in solution (ii) it does not. In this latter fluid the interfacial migrations involve boundary movement by local phase change and hence *via* the much slower stress relaxation process. The experiments of Berret *et al.* and Grand *et al.* demonstrate the very long times ($>$ 1000 s) required for stress relaxation when the shear rate very close to $\dot{\gamma}_c$. Given the coexistence of two rates of strain, one on the high shear branch and one close to $\dot{\gamma}_c$, such long fluctuation times might equally be expected in any migration of the boundary between bands, while the precise details of the positioning of the coexistence line will determine the slow fluctuation rate.

In summary we would argue that the conditions of uniform stress which prevail in the cone-and-plate rheometer result in quite complex shear band dynamics in the wormlike micelle system studied here. The characteristic timescales associated with the shear band fluctuations may be either quite short or quite long in relation to the Maxwell time, τ_M, and these dynamics are exquisitely sensitive to the precise physical chemistry of the system under study, and relatively insensitive to the startup conditions.

It is of particular interest that we have been able to see a transition, across the stability condition, in a single system, an effect which is manifest in Figures 12c and 12d. This at least means that the phenomenon can be studied somewhat independently of the chemistry. More importantly the sudden change which is manifest in this single system is strongly suggestive of an instability.

From an experimental perspective, it remains to be seen what precisely are the compositional parameters which determine the micellar dynamics. Certainly the issue of sample purity will be crucial to any meaningful comparison of experimental results between different groups. From a theoretical perspective our work raises many interesting questions concerning the physical basis for the instability of the shear band interface, the criterion which determines the stability, and the factors which govern the fluctuation dynamics?

The authors are grateful Dr. Robin Ball, Professor T.C.B. McLeish and Dr. Peter Olmsted for valuable discussions. Financial support from the Royal Society of New Zealand Marsden Fund is gratefully acknowledged.

Appendix

Pyridine (1 mole) and 1-chlorohexadecane (1.5 moles) were put into a round bottomed flask which had a reflux condenser and calcium chloride drying tube attached. The mixture was then gently refluxed for several hours. The resulting product was washed with dry acetone, and recrystallized using dry methanol and ether.

References

1. M. Doi, S.F. Edwards, J. Chem. Soc. Faraday Trans. **74**, 1789 (1978).
2. M. Doi, S.F. Edwards, *The Theory of Polymer Dynamics* (Oxford University Press, Oxford, 1987).
3. T.C.B. McLeish, R.C. Ball, J. Polym. Sci. Polym. Phys. Ed. **24**, 1735 (1986).
4. J.P. Decruppe, R. Cressely, R. Makhloufi, E. Cappelaere, Colloid Polym. Sci. **273**, 346 (1995).
5. R. Makhloufi, J.P. Decruppe, A. Ait-Ali, R. Cressely, Europhys. Lett. **32**, 253 (1995).
6. J.-F. Berret, D.C. Roux, J. Rheol. **39**, 725 (1995).
7. R.W. Mair, P.T. Callaghan, Europhys. Lett. **36**, 719 (1996).
8. R.W. Mair, P.T. Callaghan, J. Rheol. **41**, 901 (1997).
9. J.-F. Berret, G. Porte, J.P. Decruppe, Phys. Rev. E **55**, 1668 (1997).
10. M.E. Cates, T.C.B. McLeish, G. Marrucci, Europhys. Lett. **21**, 451 (1993).
11. M.E. Cates, Macromol. **20**, 2289 (1987).
12. M.S. Turner, M.E. Cates, Langmuir **7**, 1590 (1991).
13. N.A. Spenley, M.E. Cates, T.C.B. McLeish, Phys. Rev. Lett. **71**, 939 (1993).
14. M.E. Cates, J. Phys. Chem. **94**, 371 (1990).
15. J.P. Decruppe, E. Cappelaere, R. Cressely, J. Phys. II France **7**, 257 (1997).
16. J.-F. Berret, D.C. Roux, G. Porte, J. Phys. II France **4**, 1261 (1994).
17. C. Grand, J. Arrault, M.E. Cates, J. Phys. II France (submitted).
18. M.M. Britton, P.T. Callaghan, Phys. Rev. Lett. **78**, 4930 (1997).
19. P.D. Olmsted, C.-Y.D. Lu, Phys. Rev. E **56**, R55 (1997).
20. R. Rehage, H. Hoffmann, Mol. Phys. **74**, 933 (1991).
21. P.T. Callaghan, M.E. Cates, C.J. Rofe, J.B.A.F. Smeulders, J. Phys. II France **6**, 375 (1996).
22. M.M. Britton, P.T. Callaghan, J. Rheol. **41**, 1365 (1997).
23. P.T. Callaghan, Y. Xia, J. Magn. Reson. **91**, 326 (1991).
24. P.T. Callaghan, *Principles of Nuclear Magnetic Resonance Microscopy* (Oxford University Press, Oxford, 1991).
25. N.A. Spenley, X.F. Yuan, M.E. Cates, J. Phys. II France **6**, 551 (1996).
26. F. Greco, R.C. Ball, J. Non-Newtonian Fluid Mech. **69**, 195 (1997).
27. M. Cloitre, P. Perrot, J.-F. Berret, Free jets of entangled wormlike micelles, poster presentation, NATO school, *Theoretical challenges in the dynamics of complex fluids* (Cambridge University Press, Cambridge, 1996).
28. T.C.B. McLeish, J. Polym. Sci. Polym. Phys. Ed. **25**, 2253 (1987).
29. C. Liu, D.J. Pine, Phys. Rev. Lett. **77**, 2121 (1996).